Interpretation of the nitrogen isotopic signal variations in the Mauritanian upwelling with a 2D physical-biogeochemical model

Xavier Giraud, Philippe Bertrand, Véronique Garçon, Isabelle Dadou

Interpretation of the nitrogen isotopic signal variations in the Mauritanian upwelling with a 2D physical-biogeochemical model

Xavier Giraud[1] and Philippe Bertrand

Département de Géologie et Océanographie, CNRS UMR 5805 EPOC, Université Bordeaux I, Talence, France

Véronique Garçon and Isabelle Dadou

Laboratoire d'Etudes en Géophysique et Océanographie Spatiales, CNRS UMR 5566, Toulouse, France

[1] A physical-biogeochemical model is used to simulate the evolution of the $\delta^{15}N$ signal during the last glacial-interglacial transition in sedimentary cores offshore from the Mauritanian upwelling. The biological model is a classical nitrogen-based trophic chain model, which also computes the nitrogen isotope fractionation. The 2D physical primitive equation model simulates the coastal upwelling circulation and is applied for different sea level scenarios. The effect of the sea level rise, inducing the shelf immersion, seems to be a main factor explaining the organic nitrogen flux and isotopic signal variations along the last deglaciation. This effect is modulated by an upwelling seasonality that may have been much longer at the Last Glacial Maximum, around $10-11$ months instead of $4-5$ months at present. Between 15 and 5.5 kyr ago, 60% of the sedimentary $\delta^{15}N$ variations could be explained by this local shelf immersion effect. This reconstruction also reproduces the strong isotopic fall occurring between 5.5 kyr and the present.   *INDEX TERMS:* 4219 Oceanography: General: Continental shelf processes; 4255 Oceanography: General: Numerical modeling; 4267 Oceanography: General: Paleoceanography; 4845 Oceanography: Biological and Chemical: Nutrients and nutrient cycling; *KEYWORDS:* Mauritanian upwelling, nitrogen isotopes, sea level effect, fractionation, seasonality, coupled model

1. Introduction

[2] Many local studies have shown a strong relationship between core top sediment $\delta^{15}N$ and the nitrate concentration in surface water, more specifically the degree of nitrate utilization [*Altabet and François*, 1994; *Holmes et al.*, 1996, 1998]. Indeed, many processes within the biological loop discriminate between light and heavy isotopes of the nitrogen, producing a different isotopic signal for each biological variable. Particulate N and sedimentary N show variations in $\delta^{15}N$ that are directly related to the degree of nitrate utilization and the initial nitrate N isotopic composition ($\delta^{15}NO_3^-$). As this isotopic signal is produced at the sea surface and transferred to and preserved in the sediments, it constitutes an interesting paleoceanographic tracer [*Altabet and François*, 1994; *Calvert et al.*, 1995; *François et al.*, 1992].

[3] Paleoceanographic studies have shown variations of the sedimentary $\delta^{15}N$, and the most common feature is an increase of this isotopic signal from glacial to interglacial [*Farrell et al.*, 1995; *Emmer and Thunell*, 2000]. These variations have been attributed mainly to a global increase of denitrification rates in the ocean and/or a decrease of the nutrient supply through nitrogen fixation [*Altabet et al.*, 1995, 2002; *Calvert et al.*, 1992; *Farrell et al.*, 1995; *Ganeshram et al.*, 2002]. In this context, a better knowledge and understanding of this $\delta^{15}N$ proxy is directly related to the global nutrient budget, and therefore to atmospheric CO_2 changes over glacial-interglacial periods through the primary production capability [*Ganeshram et al.*, 1995; *Falkowski*, 1997].

[4] This study focuses on the record of the $\delta^{15}N$ proxy in the context of the Northwest African upwelling, where *Martinez et al.* [2000] have shown variations of the $\delta^{15}N$ signal in sedimentary cores. We investigate the impact of local effects in the formation of this signal, in opposition to external causes (global explanation with denitrification and nitrogen fixation). Concerning our study area, this external cause of variation of $\delta^{15}N$ comes from nitrates arriving in the upwelling system with a certain isotopic composition, reflecting some global patterns. In this context of upwelling, with the recycling processes, these nutrients are the input to biological processes, accompanied by isotope fractionation,

[1] Now at The Max Planck Institute for Biogeochemistry, Jena, Germany.

leading to the production of sedimentary organic matter. Finally, possible diagenetic processes may transform the latter. Moreover, the Mauritanian upwelling morphology from glacial to interglacial periods depends on the sea level and the consequent shelf immersion, modifying the recycling patterns of the upwelling.

[5] This work is a regional study, applied to the Mauritanian coastal upwelling system. Nevertheless, it addresses a reinterpretation of the local δ^{15}N record that could be a hint about a different nitrogen budget on basin or global scale.

[6] As discussed and shown by *Bertrand et al.* [2000] and *Giraud et al.* [2000], the reconstruction of the paleoconditions in the Mauritanian upwelling area becomes possible with the use of the δ^{15}N signal. The aim of the present paper is to decipher the different factors that may be responsible for the observed sedimentary δ^{15}N variations. We investigate whether the shelf width (SW) is a possible main factor, rather than global denitrification/nitrogen fixation or local diagenetic effects. More specifically, we use a physical-biogeochemical model, allowing us to model the δ^{15}N production and to reconstruct the paleoconditions prevailing in the Mauritanian coastal upwelling system. Section 2 presents the 2D physical model, used to simulate the coastal oceanic circulation, and the biological model, in which the computation of the isotopic signal is made. Section 3 presents the physical and biological structures of the upwelling in present and glacial configurations. Section 4 describes how the output of this model, the sedimentary δ^{15}N, is modulated by seasonality (SA) and nitrogen input (NI) effects, in order to be compared to the data. This comparison, leading to paleoceanographic reconstructions, is applied to two cores in the Mauritanian area in section 5. Included in this section is a discussion on the wind system that could have prevailed in this region during the Last Glacial Maximum (LGM) and the deglaciation. Section 5.4 is a sensitivity study of the fractionation parameters on the reconstructed paleoclimate scenarios and conclusions follow in section 6.

2. Models

2.1. Physical Model

[7] The physical model is the primitive equation model of *Blumberg and Mellor* [1983, 1987], in a sigma coordinate system, which incorporates the Mellor-Yamada level 2.5 turbulence closure scheme [*Mellor and Yamada*, 1982]. We use the 2D version of this model.

2.1.1. Equations

[8] This model is based on the hydrostatic primitive equations in sigma coordinates. Briefly, the equations for the 2D flow are:

$$\frac{\partial \eta}{\partial t} + \frac{\partial (uD)}{\partial x} + \frac{\partial \omega}{\partial \sigma} = 0 \tag{1}$$

$$\frac{\partial (uD)}{\partial t} + \frac{\partial (u^2 D)}{\partial x} + \frac{\partial (u\omega)}{\partial \sigma} - fvD$$
$$= -gD\frac{\partial \eta}{\partial x} - \frac{gD^2}{\rho_0}\int_\sigma^0 \left(\frac{\partial \sigma_\theta}{\partial x} - \frac{\sigma}{D}\frac{\partial D}{\partial x}\frac{\partial \sigma_\theta}{\partial \sigma}\right)d\sigma + \frac{\partial}{\partial \sigma}\left[\frac{K_M}{D}\frac{\partial u}{\partial \sigma}\right]$$
$$+ 2A_M\frac{\partial}{\partial x}\left(D\frac{\partial u}{\partial x}\right) \tag{2}$$

$$\frac{\partial (vD)}{\partial t} + \frac{\partial (uvD)}{\partial x} + \frac{\partial (v\omega)}{\partial \sigma} + fuD = \frac{\partial}{\partial \sigma}\left[\frac{K_M}{D}\frac{\partial v}{\partial \sigma}\right] + A_M\frac{\partial}{\partial x}\left(D\frac{\partial v}{\partial x}\right) \tag{3}$$

$$\frac{\partial (\sigma_\theta D)}{\partial t} + \frac{\partial (\sigma_\theta uD)}{\partial x} + \frac{\partial (\sigma_\theta \omega)}{\partial \sigma} = \frac{\partial}{\partial \sigma}\left[\frac{K_H}{D}\frac{\partial \sigma_\theta}{\partial \sigma}\right] + A_H\frac{\partial}{\partial x}\left(\frac{\partial \sigma_\theta}{\partial x}\right) \tag{4}$$

where (u, v) are the horizontal velocity components in the (x, y) directions. The coordinate system was defined with x oriented perpendicular to coast and y oriented parallel to the coast. Assuming uniformity alongshore, gradients of properties along the coast, $\partial/\partial y$ are null. The free surface elevation is $\eta(x,t)$, $D = H + \eta$, $H(x)$ is the bottom topography, $\sigma = (z - \eta)/D$, z is the conventional Cartesian vertical coordinate, t is time, ω is the velocity component normal to σ surfaces, σ_θ is the potential density, ρ_0 is a constant reference density, f is the Coriolis parameter, and g is the acceleration of gravity. The vertical kinematic viscosity K_M and diffusivity K_H are given by the computation of the turbulent kinetic energy and a turbulence length scale, solutions of the equations of the turbulence submodel [*Allen et al.*, 1995; *Mellor and Yamada*, 1982]. A_M is the horizontal kinematic viscosity and is calculated by the Smagorinsky diffusivity scheme with constant $C = 0.2$, and A_H ($=A_M/10$) is the horizontal heat diffusivity. For details of the full, 3D version of the ocean model refer to the work of *Blumberg and Mellor* [1983, 1987] and *Mellor* [1998].

2.1.2. Model Domain and Boundary Conditions

[9] The σ levels vary from $\sigma = 0$ at the surface [$z = \eta(x,t)$] to $\sigma = -1$ at the bottom [$z = -H(x)$], with a logarithmic distribution in the top and bottom and a linear distribution in between. This distribution is used to obtain well-defined surface and bottom boundary layers. The coordinate system is positive onshore (x) and northward (y), with $x = 0$ at the offshore boundary.

[10] The eastern boundary is a coast, with a zero flow across the boundary. The open western boundary specification is a radiative boundary condition. The wind stress is specified at the surface, but no buoyancy forcing was used in this set of paleoceanographic experiments. The flow at the bottom grid point, half a grid cell below the seabed, is set to zero.

2.1.3. Time Step, Parameterization, and Model Initialization

[11] The horizontal grid size is $\Delta x = 2$ km, for a domain width of 344 km, and the vertical grid totals 30σ levels, with six intervals within a logarithmic distribution for both bottom and surface layers. The depth at the coast is 10 m. In the initial interglacial configuration, the SW is 136 km large, with a depth of 100 m at the shelf break, and the depth offshore, after the slope, is 3060 m.

[12] Finite difference time steps are 180 s for the baroclinic (internal mode) and 6 s for the barotropic (external mode) components. The reference density is $\rho_0 = 10^3$ kg m^{-3} and $f = 10^{-4}$ s^{-1}. The initial temperature and salinity fields correspond to a uniform and stratified ocean. Initial velocities are null. The upwelling is initiated by a gradual
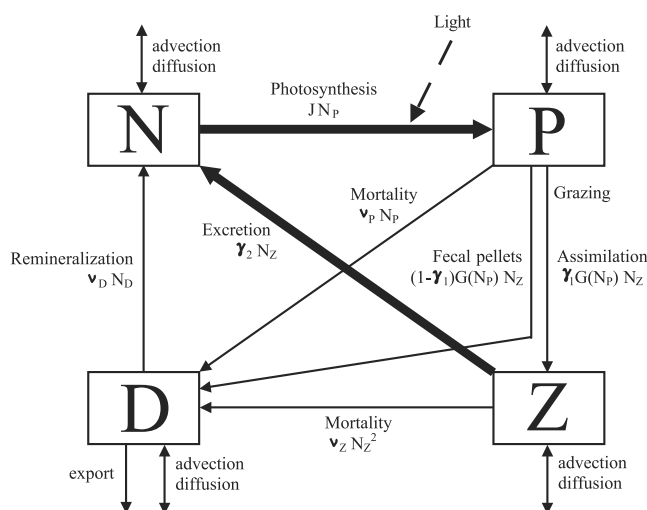
Figure 1. Scheme of the biological model [adapted from *Oschlies and Garçon*, 1999; *Giraud et al.*, 2000]. Parameters of fluxes between nutrients (N), phytoplankton (P), zooplankton (Z), and detritus (D) are given in Table 1. Bold arrows represent the two main important isotope fractionation processes considered, i.e., phytoplankton photosynthesis and zooplankton excretion.

increase of the wind stress intensity from 0 to 10^{-4} m^2 s^{-2} over 1.25 days and held constant for the remainder of the simulation. The wind is directed southward.

2.2. Biological Model

2.2.1. Initial Model

[13] The biological model must accommodate contradictory constraints. First, it must be able to compute the isotopic signal of each variable and to take into account the different paths of fractionation along the trophic food chain. Second, we have to minimize its complexity, because of the computation time cost. We use the model described by *Giraud et al.* [2000], which has already been applied in a coastal upwelling environment. The model is a classical nitrogen-based one, with four components: nutrients (N), phytoplankton (P), zooplankton (Z), and a detritus pool (D) (Figure 1). The computation method of the nitrogen fractionation used by *Giraud et al.* [2000] leads to a doubling of the state variables. It therefore justifies the use of a simple four state variable biological model.

[14] This fractionation model includes two ways of nitrogen differentiation. During photosynthesis, an enrichment factor associated with the nitrate uptake exists. When nitrate is used as the substrate by phytoplankton, the resulting new living particulate organic matter is depleted in ^{15}N as compared to the nitrate pool. Field and laboratory studies invoke different fractionation factors [*Sigman et al.*, 1999]. For this study, we chose the value presented by *Waser et al.* [1998]: the newly formed biomass is about 5.2‰ lower than the initial nitrate. A sensitivity case study of this parameter follows in section 5.4.

[15] The second fractionation path occurs during the zooplankton excretion, where zooplankton keeps preferably

the heavy nitrogen isotope (^{15}N). Nitrogen isotope fractionation by zooplankton during excretion is therefore responsible for the stepwise enrichment of ^{15}N along the trophic food chain, in our case between phytoplankton and zooplankton. As a result, zooplankton is about 3.4‰ heavier in δ^{15}N than phytoplankton [*DeNiro and Epstein*, 1980; *Minagawa and Wada*, 1984]. Fractionation parameters are kept identical as in the model of *Giraud et al.* [2000]. This means that we do not consider any bacterial remineralization fractionation in order to keep the ecosystem structure of the model simple. In the sensitivity case study of section 5.4, we will, however, investigate the effect of such a fractionation. Denitrification in the water column is not considered because oxygen concentrations in our area, the Mauritanian margin, are too high for nitrate reduction to occur [*Minas et al.*, 1982]. Another fractionation may occur during the formation of fecal pellets produced by the marine zooplankton. As the difference between the fecal pellets δ^{15}N and the animal δ^{15}N ranges between -3.7 and 4.8‰ for different zooplankton classes [*Montoya*, 1994], we will not consider this fractionation process. A last possible signal transformation would be a diagenetic effect in the sediments. But at present, little diagenetic effect has been observed [*Altabet and François*, 1994], and *Martinez et al.* [2000] did not find any significant down core changes in δ^{15}N in the first centimeters of sediment in our study area. However, we do not exclude such a late process in sediment, and this could be invoked to explain a part of the shift between the model output and the sedimentary data. But the purpose of this study is focused on the column water processes and aims to quantify the shelf immersion effect.

2.2.2. Initial Conditions and Parameters

[16] The biological fields are initiated with a low concentration of nitrates in the surface layer, and 10 mmol N m^{-3} in the deep waters. Their isotopic signature is set to 6.2‰, which has been cited as the value for the deep ocean nutrients [*Altabet and Curry*, 1989; *Liu and Kaplan*, 1989; *Montoya*, 1994]. This value is only assigned for the calculation, and whatever the real isotopic value of nutrients in the North Atlantics is, the δ^{15}N of the incoming nutrients in the Mauritanian coastal upwelling system during the last deglaciation is a reconstructed parameter of the following paleoceanographic scenarios.

[17] Initial values of phytoplankton, zooplankton, and detritus are set to 2.0, 0.2, and 0 mmol N m^{-3}, respectively. Primary production, together with mortality and zooplankton grazing, control the evolution of the phytoplankton population. Zooplankton excretion and remineralization of detritus regenerate the nutrient supply.

[18] Three minor changes are introduced, as compared to the work of *Giraud et al.* [2000]. In the photosynthesis formulation, we consider the light attenuation due to seawater and to phytoplankton concentration itself. These parameters are chosen to reproduce a euphotic layer depth of about $20-30$ m, characteristic of the Mauritanian upwelling region [*Babin et al.*, 1996; *Morel*, 2000] (see Table 1 and Appendix A).

[19] Modeled surface concentration of phytoplankton and primary production, forced by the 2D physics, were too small compared with typical values in the Mauritanian

Table 1. Parameters of the Biological Model[a]

Parameter	Symbol	Value
Phytoplankton Coefficients		
Initial slope of *P-I* curve	α, (W m^{-2})$^{-1}$ d^{-1}	0.025
Light attenuation due to water	k_w, m^{-1}	0.1
Light attenuation by phytoplankton	k_c, m^{-1} (mmol m^{-3})$^{-1}$	0.03
Maximum growth rate parameters	a, d^{-1}	0.6
	b	1.066
	c, (°C)$^{-1}$	1.0
Half-saturation constant for N uptake	k_1, mmol m^{-3}	0.5
Specific mortality rate	ν_P, d^{-1}	0.03
Zooplankton Coefficients		
Assimilation efficiency	γ_1, d^{-1}	0.75
Maximum grazing rate	g	1.0
Prey capture rate	ε, (mmol m^{-3})$^{-2}$ d^{-1}	1.0
Quadratic mortality[b]	ν_Z, (mmol m^{-3})$^{-1}$ d^{-1}	0.2
Excretion	γ_2, d^{-1}	0.03
Detrital Coefficients		
Remineralization rate	ν_D, d^{-1}	0.05
Sinking velocity	ω_D, m d^{-1}	25

[a]From [*Oschlies and Garçon*, 1999]. Parameters have been adjusted for the upwelling system.

[b]Zooplankton quadratic mortality term represents increasing populations of predators as zooplankton populations increase and is more stable than a linear term [*Steele and Hederson*, 1992; *Evans*, 1999].

upwelling (see section 3.1 for typical values) due to an extremely high pressure of zooplankton grazing. The influence of the zooplankton grazing upon the phytoplankton growth in an upwelling system is important because the zooplankton concentration is on the same order as the phytoplankton concentration [*Gunson et al.*, 1999]. In this upwelling context, a satisfying phytoplankton growth is obtained by limiting the zooplankton activity. This is the reason why the formulation of the model has been changed compared to the initial parameterization adopted for the entire North Atlantic Ocean [*Oschlies and Garçon*, 1999]. The zooplankton maximum grazing rate has been diminished to a value of 1 d^{-1} (used by *Sarmiento et al.* [1993] and *Fasham* [1995]) to restrain its pressure on the phytoplankton.

[20] In the upwelling regions, the particulate organic matter can be of large size, and this leads to large sinking velocities. However, the biological model considers only one class of detritus. The vertical velocity of sinking particles is set to 25 m d^{-1} [*Alldredge and Gotschalk*, 1988; *Wefer and Fischer*, 1993].

2.3. Coupling Between Physics and Biology

[21] This biological model is coupled to the physical one. All the ecosystem components are transported by advection and diffusion. For any biological state variable of concentration N_i, the equation is as follows:

$$\frac{\partial N_i D}{\partial t} + \frac{\partial N_i U D}{\partial x} + \frac{\partial N_i w}{\partial \sigma} = \frac{\partial}{\partial \sigma}\left[\frac{K_H}{D}\frac{\partial N_i}{\partial \sigma}\right] + \frac{\partial}{\partial x}\left(H A_H \frac{\partial N_i}{\partial x}\right)$$
$$+ \text{SMS}(N_i), \qquad (5)$$

where SMS is the source minus sink term corresponding to the biological interactions of the food web model [*Giraud et al.*, 2000]. For the definitions of other parameters, see section 2.1. The expression for detritus transport includes an

additional sinking term ($-\omega_D(\partial N_D/\partial \sigma)$), where ω_D is the vertical sinking velocity of particles.

2.4. Offline Mode and Sea Level Variations

[22] The model has to be run on a reasonably long period to ensure a good distribution of the biological fields and particularly of the nitrogen isotopes, in order not to record a transient situation. However, a long running time of the 2D physical model would erase the main features of the upwelling, which would evolve toward a homogeneous field (continuous entry of cold waters in the deep and exit of the overlying warm waters).

[23] The biological model is therefore run in an offline mode: the oceanic circulation is first determined and then used to force the evolution of the biological fields. Runs are performed to obtain characteristic circulation schemes for the different sea level scenarios. All parameters being equal, the only change is the sea level from modification of the SW. The simulation period for the physical model is 75 days long. In order to smooth the circulation pattern and to avoid short timescale variability, a mean of the circulation field for period from days 45 to 75 is subsequently used to compute advection of the biological variables. The upwelling index (UI) is defined as the sea surface temperature difference between coastal areas and the offshore zone. With this method, the UI is about 4.5°C, which is a mean value for the Mauritanian coast [*Mittelstaedt*, 1991]. As we cannot estimate this index for the glacial period, we use the same wind conditions for each sea level scenario, and we stop the circulation scheme after the same duration.

2.5. Sedimentary Production

[24] Biogenic particles sink through the water column. Some of them undergo total remineralization while others eventually reach the sediments before complete remineralization. Before their definitive fossilization, many other processes may occur, including resuspension, advection, gravity processes of sediments, and diagenesis. Only a "sedimentary model" coupled with the circulation model could represent these mechanisms. In order to parameterize them, two transformations are applied to the sedimentary signal.

[25] Under the action of resuspension processes, the organic matter arriving on the shelf is transported to and accumulates on the slope, between 1000 and 2000 m depth, in a zone called the slope depocenter [*Fütterer*, 1983]. We therefore consider that the fossilized sediment existing at any location can result from all the sedimentation processes occurring between the coast and that point. One first transformation is to consider the upstream cumulative sedimentation for reconstructing the sedimentary signal.

[26] To consider any loss of particulate organic nitrogen by resuspension or diagenesis, we apply a correction factor. We have divided sedimentary organic nitrogen fluxes (ONF) of the model output by 12.5×10^3. This means that we consider that around 0.08‰ of the sediments stays definitively fossilized. This correction factor is considered constant along the glacial-interglacial transition. However, as this factor includes gravity processes, it may have changed with the sea level and the related immersion of the shelf. It could

also be different from one location to another, considering local particularities of the slope and continental shelf topography. This correction factor is therefore a key uncertainty of the following paleoceanographic reconstructions.

3. Physical and Biological Structures

3.1. Interglacial Period

[27] Vertical sections of temperature, cross-shore velocity, nutrients, and phytoplankton concentrations, and nitrate $\delta^{15}N$ are shown in Figure 2 for a high sea level configuration (SW of 128 km). The temperature distribution in Figure 2a shows the upwelling of cold deep waters on the shelf. At the upwelling emergence zone, the surface temperature minimum is around 16.5°C, while the offshore surface water temperature is 21°C. The UI is therefore 4.5°C. This invasion of the shelf is clearly visible with the cross-shore velocities section (Figure 2b). The surface current is directed offshore ($U_{max} = -10.1$ cm s^{-1}) and a compensating current flowing toward the coast forms a bottom boundary layer ($U_{max} = 11.1$ cm s^{-1}). These currents correspond to a recirculation cell developing on the shelf.

[28] These physical structures force the distribution of the biological variables. In Figure 2d, the modeled phytoplankton is mostly distributed on the shelf and in the upper layer, and reaches a first maximum concentration around the midshelf, where cold, nutrient-rich waters upwell. The boundary between the coast, where phytoplankton is poorly present, and this upwelling region is the primary front. Even if phytoplankton growth is limited to the euphotic layer (about 20 m), phytoplankton is transported down to 100 m by advection and mixing. Because of detritus remineralization and strong recycling, nutrients also reach high concentrations in the midshelf area, around 12 mmol N m^{-3} (Figure 2c). Detritus are largely produced by mortality of both phytoplankton and zooplankton, and regenerate the nutrient pool by remineralization. Offshore from the coldest surface water temperature point, phytoplankton concentration slightly decreases due to mortality and zooplankton grazing. Nutrients become depleted during the offshore transport, and detritus concentration decreases because of remineralization and sinking. At the shelf break location, a secondary front appears. Vertical velocities provide a supply of nutrients to the surface layer, resulting in a second maximum of phytoplankton concentration. This is also another location of important detritus production. Once again, the system evolves offshore toward oligotrophy.

[29] Thus the model reproduces realistic chlorophyll concentrations and primary production in the surface layer. Maximum values for chlorophyll concentrations in the Mauritanian upwelling are up to 3.5 mg Chl-a m^{-3} [Fischer et al., 1996; Gabric et al., 1993; Morel, 2000], corresponding to a phytoplankton concentration of 2.2 mmol N m^{-3} (with a Chl-a/N ratio of 1.59 mg Chl-a (mmol N)$^{-1}$ [Oschlies and Garçon, 1999]). Primary production ranges from 1.5–2 g C m^{-2} d^{-1} in the eutrophic zone to 0.29 g C m^{-2} d^{-1} in oligotrophic sites [Morel, 2000]. Simulated primary production in interglacial configuration ranges between 0.1 and 1.5 g C m^{-2} d^{-1}. Primary production in oligotrophic regimes is underestimated, however, it will not have any important impact on the sedimentary signal

production, which is mostly determined from the eutrophic regime on the continental shelf.

[30] Figure 2e presents the isotopic signal of nitrate. In agreement with the nitrate distribution, higher values appear in nutrient-depleted regions, at the surface layer, and offshore of the shelf break.

3.2. Glacial Period

[31] The glacial configuration, with a low sea level, is presented in Figure 3. As the sea level is below the shelf break, no shelf exists, which greatly modifies the oceanic circulation. The cold deep waters upwell at the coast (Figure 3a), and there is no recirculation cell. The UI is now about 7°C, which is stronger than in the previous case. Currents are directed offshore in the surface layer ($U_{max} = -6.1$ cm s^{-1}) and shoreward below ($U_{max} = 2.7$ cm s^{-1}; Figure 3b). Deep waters with high concentrations of nitrates reach the surface at the coast (Figure 3c). Maximum surface nitrate concentration is around 10 mmol N m^{-3}. During the offshore transport by the surface currents, nutrients are consumed by the phytoplankton. The maximum nutrient concentration is followed by the maximum phytoplankton concentration (0.96 mmol N m^{-3}), followed by zooplankton development. The high nitrate concentrations in the surface mostly come from subsurface water upwelling rather than from detritus remineralization.

[32] According to this distribution of the nutrient concentrations, the $\delta^{15}N$ of nitrates in the surface layer increases offshore from the coast. High values are reached far from the coast and from the sedimentary core location. The organic matter produced near the upwelling emergence zone comes from nutrients with light $\delta^{15}N$ values and records the first changes in the nitrate uptake.

[33] The expectation of higher $\delta^{15}N$ values far from the coast is reproduced by the model for both situations of high and low sea level. This increase of isotopic record is confirmed by surface core studies from Martinez et al. [2000]. They have shown an increase of the $\delta^{15}N$ values in surface sediment in a transect in front off Cape Blanc. Values are increasing while going offshore.

[34] The modification of topography due to the sea level variation has a major role on the circulation mode. Between the two typical configurations of high and low sea level scenarios (Figures 2 and 3), differences in the biological development come from the degree of recycling of the biological variables, and in particular, the detritus. As shown in the next section, this will have consequences on the isotope cycle and sedimentary signal, because it could explain how to produce low $\delta^{15}N$ in both situations of low and high sea level, and higher values in intermediate situations.

4. Sensitivity of $\delta^{15}N$ to Different Physical and Biogeochemical Processes: Numerical Experiments

[35] This part aims to stress and illustrate the possibility of getting different responses ($\delta^{15}N$ and ONF) from different combinations of physical and biogeochemical processes.

4.1. Basic Experiment: Sea Level Effect

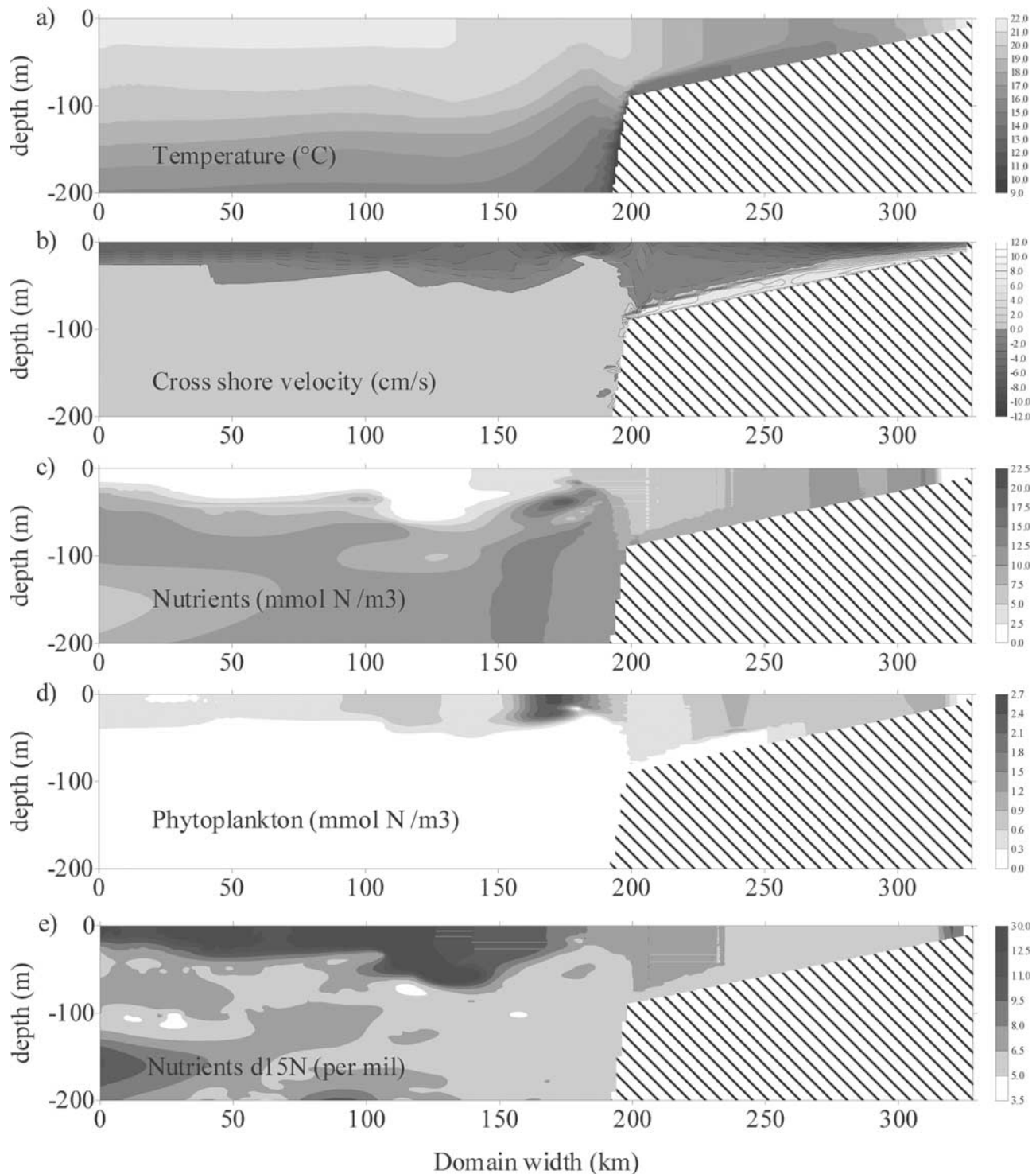[36] The basic experiment consists in running the model in different sea level scenarios to obtain the

Figure 2. Cross section of (a) temperature (in °C), (b) cross-shore velocity (in cm s^{-1}, positive values indicate currents directed onshore), (c) nutrients and (d) phytoplankton concentrations (in mmol N m^{-3}), and (e) nitrate δ^{15}N (in ‰) for a high sea level scenario (SW of 128 km).

corresponding signal for a virtual coring site located about 50 km offshore of the shelf break, which would correspond to the mean position of the studied cores. Each configuration is thus determined by the SW, evolv-ing between 0 km (glacial period) and 136 km (inter-glacial period). Figure 4 presents the evolution of the isotopic signal and ONF in the sediments for each of these SW situations.
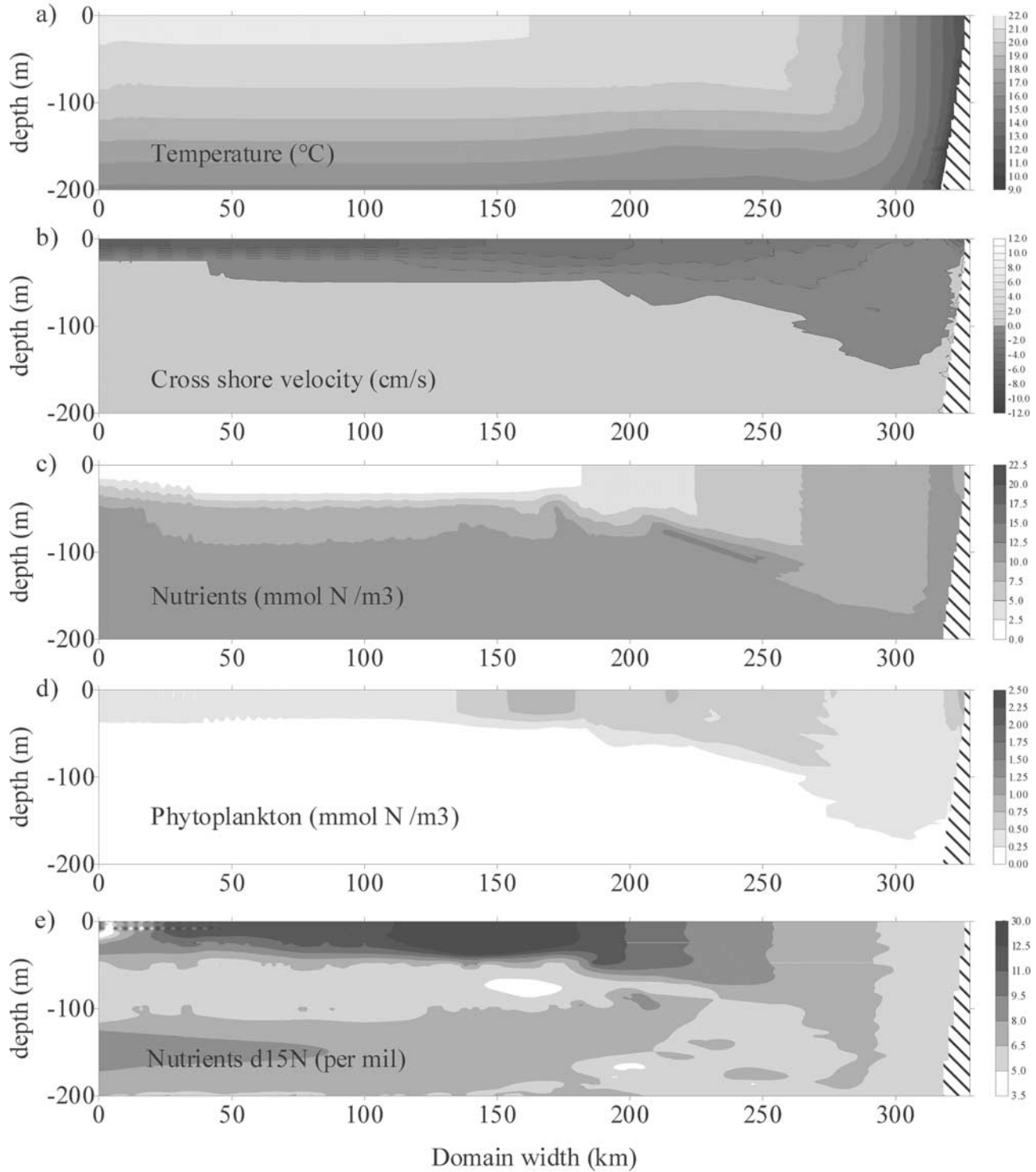
Figure 3. Cross section of (a) temperature (in °C), (b) cross-shore velocity (in cm s⁻¹, positive values indicate currents directed onshore), (c) nutrients and (d) phytoplankton concentrations (in mmol N m⁻³), and (e) nitrate δ^{15}N (in ‰) for a low sea level scenario (no continental shelf).

[37] For the situation without a continental shelf (0 km of SW), the sediments reaching the core site are characterized by a low ONF associated with a low δ^{15}N (0.27 mmol N cm⁻² kyr⁻¹, 1.73‰). In this situation, the core site is close to the coast, where the biological system is not yet well developed. The export production is low (low flux of organic matter reaching the sediments) and the isotopic signal corresponds to the initial nitrate value (6.2‰)
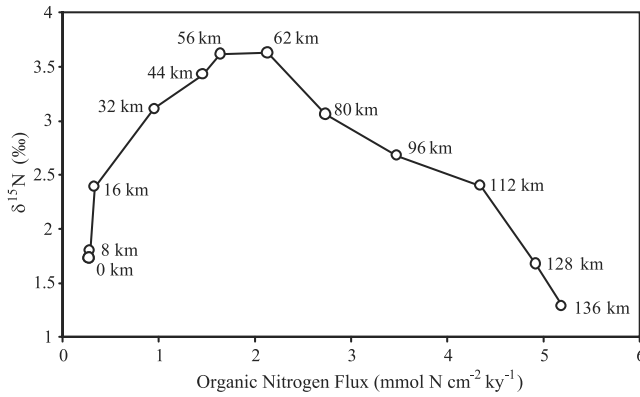
Figure 4. Sedimentary output signal of the model for the different SW configurations. The SW varies between 0 and 136 km.

affected by the first steps of phytoplankton growth ($\varepsilon = -5.2‰$).

[38] With increasing SWs (sea level rise and shelf immersion), two major changes are observed:

[39] (1) For the narrow SWs, from 0 to 56 km, a rapid increase of the isotopic signature coincides with a moderate increase of the ONF.

[40] The recirculation cell appearing on the outer shelf due to the sea level rise is small and produces a moderate increase of the cumulated sedimentary biogenic nitrogen flux, as well as a strong isotopic fractionation. As this recirculation cell becomes larger, the effects of recycling and fractionation by the zooplankton becomes more important and the isotopic signal increases. The maximum $\delta^{15}N$ is 3.63‰ (for an initial nitrate value of 6.2‰).

[41] (2) For larger SWs, the pattern is reversed for the isotopic signal. While the SW continues to increase, the ONF increases rapidly, due to increasing cumulated production, but the sedimentary $\delta^{15}N$ decreases. As explained by *Bertrand et al.* [2000], the large SW induces a strong recycling of detritus and increases the supply of regenerated nutrients. This excess of nutrients limits the depletion of this pool, which retains its initial low isotopic value longer. Thus the detritus pool has low $\delta^{15}N$ values. The cumulative organic nitrogen production is important, due to the large shelf extension.

4.2. Seasonality Effect

[42] Here we want to formulate and consider the importance of the SA on the production of the sedimentary signal (ONF and isotopic composition).

[43] The previous values obtained for the basic experiment correspond to a constant upwelling, present over a full year. The upwelling is thus active during 12 months: its SA, here defined as the number of months the upwelling is active, is 12. The sedimentary ONF of the basic experiment (ON_BE), produced over a full year, can be expressed as a function of the SW, as shown in Figure 4:

$$ON_{BE} = f_1(SW, SA = 12). \tag{6}$$

[44] In fact, the upwelling is not always active and the SA should be reduced. For an equivalent SW situation, a shorter-activity duration (a shorter SA) will induce a decrease of the ONF, without changing the corresponding isotopic signal. This can be translated by the following equation, relating the ONF of the data (ON_DATA) to the modeled ONF ON_BE:

$$ON_{DATA} = f_2(SA, ON_{BE}) = \frac{SA}{12}ON_{BE}. \tag{7}$$

Figure 5 shows different curves obtained while reducing the SA from the basic experiment.

[45] Presently, the upwelling activity is almost permanent at 21°N, the location of the core 11K, offshore of Cape Blanc, but reinforced during 5–6 months [*Mittelstaedt*, 1991; *Speth and Detlefsen*, 1982]. At 25°N, the maximum upwelling period is less pronounced, lasting 4–5 months.

[46] Both locations (north and south) are under the influence of the Inter Tropical Convergence Zone (ITCZ), which acts on the wind intensity and direction, relative to the coastline orientation. The more the wind is parallel to the coast, the more efficient the Ekman transport is.

[47] All these parameters may have changed during the glacial-interglacial transition. The sea level variation changed the shelf extension but also redrew the coastline orientation (Figure 6). The ITCZ latitudinal migration from summer to winter may have been less extended during the glacial period [*Leroux*, 1993], and this effect will be discussed in section 5.3.

4.3. Nutrient Input Effect

[48] The starting point of the isotopic signature in the biological food web is the $\delta^{15}N$ of the nutrients that upwell on the shelf. In the basic experiment, we set this value at 6.2‰ (see section 2.2.2), so the NI is 6.2. The sedimentary isotopic signal of the basic experiment ($\delta^{15}N_{BE}$), produced with NI = 6.2, can be expressed as a function of the SW, as shown in Figure 4:

$$\delta^{15}N_{BE} = f_1(SW, NI = 6.2). \tag{8}$$

[49] This NI value may vary on regional scales or may have changed during the glacial-interglacial transition. Any variation of the isotopic signature of NI has a direct consequence on the resulting $\delta^{15}N$ in the sediments, and this result can be translated into the following equation,
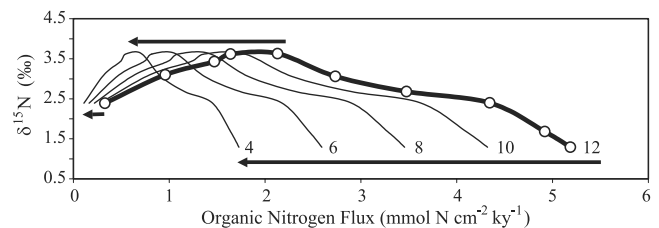

Figure 5. The SA effect. The curve of the basic experiment corresponds to a SA of 12 months. Other curves correspond to different situations with reduced SA (10, 8, 6, and 4 months).
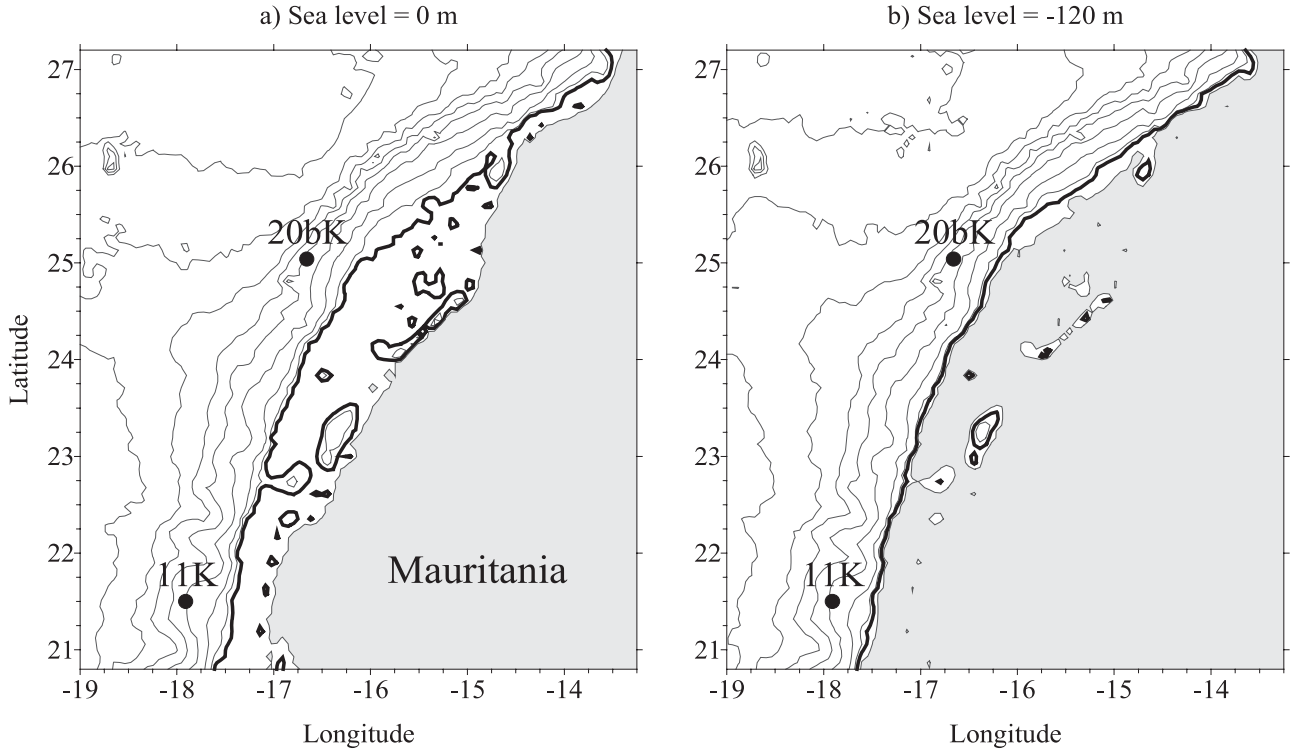
a) Sea level = 0 m

b) Sea level = -120 m

Figure 6. (a) Bathymetry of the Mauritanian coast for the actual sea level with the location of the cores 11K and 20bK. (b) Map of the LGM; a representation of the same topography with a sea level 120 m lower. The bold line is the 100 m isodepth.

relating the isotopic signal of the data ($\delta^{15}N_{DATA}$) to the modeled isotopic signal $\delta^{15}N_{BE}$:

$$\delta^{15}N_{DATA} = f_3(NI, ON_{BE}) = \delta^{15}N_{BE} + (NI - 6.2). \quad (9)$$

[50] Figure 7 shows different curves obtained while changing the nutrient input. An increase of the NI signature induces an equivalent increase of the basic experiment $\delta^{15}N$, without changing the ONF (SA and SW are held constant).

4.4. Biological Effect: Fractionation Factors

[51] Two sensitivity tests are carried out in order to evaluate the impact of the variability of the fractionation factors observed in many studies [*Montoya*, 1994; *Sigman et al.*, 1999]. First, we changed the fractionation factor of nitrate uptake from 5.2 to 3.2‰. In a second test, we added a fractionation process ($R_m = 1‰$) to the remineralization path. The process to produce the sedimentary signal (ONF and isotopic signal) in relation to increase in SW is the same as for the initial experiment, and the resulting curves are presented in Figure 8.

[52] Changing the fractionation parameter associated with the nitrate uptake has a slightly constant effect for glacial or interglacial simulations: by decreasing the fractionation factor from 5.2 to 3.2‰, it increases the resulting sedimentary production to a range between 0.9 and 1.73‰ (Figure 8, gray circles). Thus the evolution of the sedimentary signal keeps the same trend as previously described for the basic experiment. This bell shape shows an increasing

ONF with an increasing SW, first an increasing isotopic signal for short SWs, then a decreasing $\delta^{15}N$ for larger continental shelves' configurations.

[53] The second sensitivity test is the addition of a fractionation factor associated with the remineralization loop. We have added a 1‰ fractionation. Here again, the resulting sedimentary production has the same pattern for the glacial-interglacial evolution (Figure 8, black circles), keeping this characteristic bell shape. Compared to the initial curve, the result is between 0.6 and 1.65‰ higher.
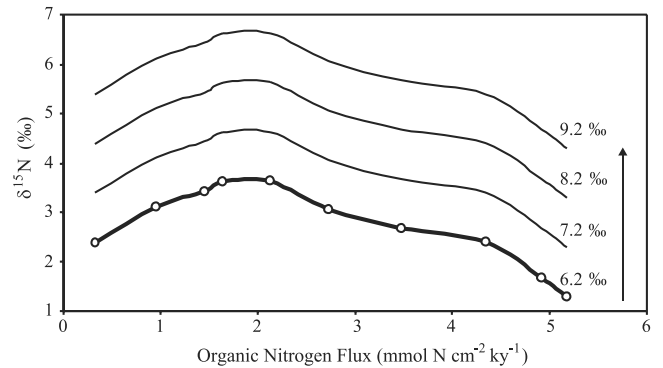

Figure 7. The NI effect. The curve of the basic experiment corresponds to NI = 6.2‰. Other curves correspond to different situations with increasing deep nutrient isotopic signature (NI = 7.2, 8.2, and 9.2‰).

[54] In conclusion, as shown in Figure 8, both sensitivity tests demonstrate that changing the fractionation factors has a strong impact on the sedimentary signal, all other parameters being equal. But this effect is constant over the different SW configurations. The value of the fractionation factors is important to explain the formation of the sedimentary $\delta^{15}N$ signal, but as this effect is roughly constant over the glacial to interglacial transition, it cannot explain the variations of this signal.

4.5. Effect of the Wind Intensity

[55] Some studies invoke an increase of the wind intensity at the LGM in Northwest Africa [e.g., *Sarnthein et al.*, 1981; *Leroux*, 1996; *Martinez et al.*, 1999]. The expected effect of this higher wind intensity should be an intensification of the upwelling, i.e., the flux of subsurface water upwelled to the surface. The associated nutrient supply to the euphotic layer should amplify the primary production, and therefore the first consequence of the increase of the wind intensity should be an increase of the ONF to the sediments. But there is another process associated with the wind intensity. It should also increase the surface current velocity. The water masses should be transported offshore more rapidly, and the export of the primary production would occur on a larger area, and more offshore compared to the continental shelf. This second effect of the increase of the wind intensity would counteract the previous one, by decreasing the nitrogen organic flux to the core location.

[56] In conclusion, the effect of the increase of the wind intensity is difficult to estimate because of the opposite consequences explained previously. For the following attempt of reconstruction in section 5, we will consider a neutral effect of this wind intensity. This should be treated more accurately with a full 3D physical model in further studies.

4.6. Summary and Conclusion of the Physical and Biogeochemical Effects

[57] In conclusion, we can summarize the importance of each process on the formation of the sedimentary signal for both $\delta^{15}N$ and ONF. The sea level effect cannot be ignored, and draws the main pattern of the isotopic signal during the glacial-interglacial transition. It influences both the $\delta^{15}N$ and ONF. The nutrient input effect is important as well because it directly affects the sedimentary $\delta^{15}N$ signal in the same range as its initial variation. But it does not act on the ONF. The biological effect associated with the fractionation factors has the same kind of consequence. It affects only the $\delta^{15}N$ signal. However, as previously said, it cannot be responsible for glacial-interglacial variations. At last, the SA effect is important because it modifies the ONF, without changing the isotopic signal. It is also interesting to note that the SA effect is more important when the SW is larger.

5. Attempt of Reconstruction of Mauritanian Cores Signal

[58] This part is an attempt to apply the previous conclusions about the formation of the nitrogen isotopic signal in a coastal upwelling system. It aims as well to indicate
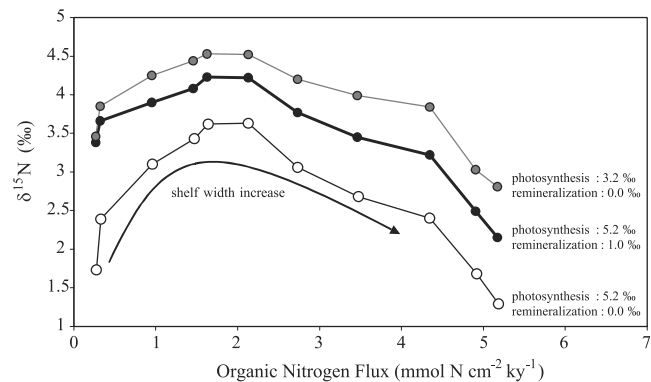

Figure 8. Model outputs of isotopic $\delta^{15}N$ signal (‰) and ONF (mmol N cm^{-2} kyr^{-1}) as a function of the SW evolution for different configurations of fractionation factors (Nu, fractionation factor for nitrate uptake; Rm, fractionation factor for remineralization). Open circles: Nu = 5.2‰, Rm = 0‰ (curve of Figure 4); black circles: Nu = 5.2‰, Rm = 1‰; shaded circles: Nu = 3.2‰, Rm = 0‰.

how to go toward a reconstruction of the conditions prevailing to the formation of this sedimentary signal.

5.1. Distinct Feature of the Two Cores and Strategy of Reconstruction

[59] The two cores of the Mauritanian margin of interest here, the core 11K, offshore of Cape Blanc (21°28.87′N; 17°57.35′W; 1200 m depth), and the core 20bK (25°1.7′N; 16°39.2′N; 1450 m depth) were collected during the SEDORQUA cruise (Figure 6). They show the same trend for $\delta^{15}N$ down core measurements, i.e., an increase during the deglaciation [*Martinez*, 1997] (Figure 9). However, the core 11K shows a peculiar feature after the climatic optimum: from 7.7 to 1.1 kyr, the isotopic signal decreases (Figure 9). In contrast, data of cores 11K and 20bK have different patterns for the ONF. The ONF of the core 20bK decreases during the glacial-interglacial transition while it increases for the core 11K. Thus on a plot of isotopic signal versus ONF, the two core-data have crossed features (Figure 9).

[60] Figure 10 shows how each sedimentary data point can be reconstructed from the basic experiment curve (Figure 4), modified with the equations of SA and NI effects (equations (7) and (9)) described in the previous section.

[61] The following strategy consists in determining the relative importance of sea level, SA, and NI in the production of the signal of sedimentary core. Considering that for each data point we have a system of two equations (equations (7) and (9)) and three variables (SW, SA, and NI), the system has one degree of liberty. For both cores (11K and 20bK), we set a SW evolution. This choice reduces the number of variables to two (SA, NI), and the system can now be solved. The validity of each scenario is discussed hereafter.

[62] In order to establish these scenarios, we have to evaluate the range of each of these varaibles (SW, SA, and NI) and how constraint is the problem. It is important to remind that during the last deglaciation, the continental margin was affected by a major event: the sea level rise
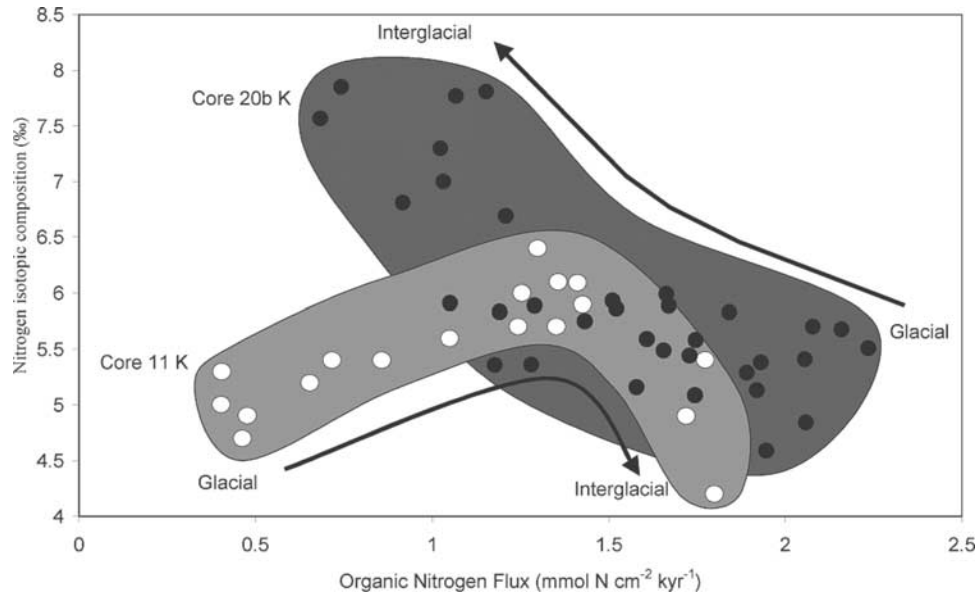
Figure 9. Sedimentary data for cores 11K and 20bK: $\delta^{15}N$ versus ONF. Data is from *Martinez* [1997]. Arrows show the evolution during the deglaciation.

and the shelf immersion. This process and its effect on $\delta^{15}N$ cannot be overlooked. Our previous results, section 4.1 and Figure 4, show that this effect reflects most of the variations recorded by core 11K. Looking carefully at the map of the Mauritanian margin (Figure 6), we can evaluate the shelf immersion history during the deglaciation. The sea level evolution is relatively well known [*Bard et al.*, 1996]. It consists of a regular increase from the LGM to 6 kyr BP, followed by a slightly constant situation. Presently, the northern core 20bK is located near a shelf about 150 km wide, while the southern core 11K is in front of a narrower continental shelf (about 40 km). However, if we consider the southward currents existing close to the coast, the material arriving at any location may originate from a more northeasterly area. The existence of these currents and their possible variations due to topographic and climatic changes, make the effects of the immersion less constrained. This led us to perform the reconstruction of the scenarios in terms of SW rather than in terms of sea level evolution. This SW parameter will therefore represent the extension of the continental shelf responsible for the production of the material arriving on the slope, taking into account not only the morphology of the shelf but also the current transport effects.

[63] If we consider the topography for the LGM (sea level 120 m lower, Figure 6b), the shelf facing the core 11K location disappears. This is due to the fact that the shelf break is at 100 m in the southern part of this coast (in front of core 11K, Cape Blanc). In contrast, the shelf break is deeper (at around 200 m depth) in the northern part of this margin. While decreasing the sea level of 120 m, a shelf is still present in front of the core 20bK, and can participate in an active upwelling recirculation cell. We will therefore choose scenarios where the SW increases during the deglaciation for core 11K and remains constant for core 20bK.

[64] SA is known for the present period. It is 4–5 months per year at core location 11K, and less for core 20bK. By

definition, it must be lower than 12 months for the reconstructions, which limits the solution possibilities. To evaluate minimum and maximum local effects of SW immersion on the sedimentary isotopic signal, we will test scenarios minimizing the NI variations, which are considered here as an external cause of the sedimentary nitrogen isotopic signal variations.

5.2. Reconstruction for Core 11K

[65] The history of the data signal ($\delta^{15}N$ and ONF) for core 11K can be divided into four parts (Figure 11a). From 20 to 15 kyr, the isotopic signal and the ONF are low and almost stable. From 15 to 11 kyr, both increase, and then are stable again until 5.5 kyr. From 5.5 kyr to present, the signals diverge: the isotopic signal falls from 6.1 to 4.2‰,
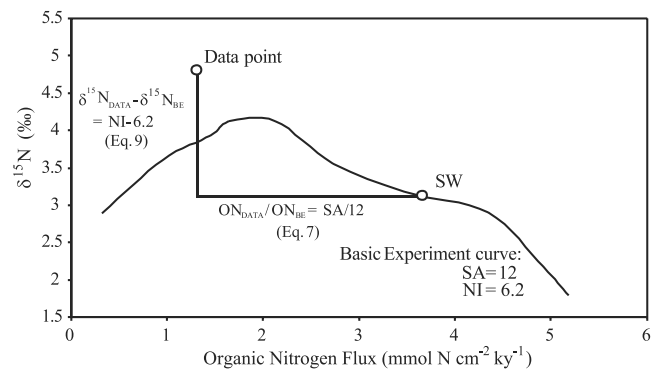

Figure 10. Relation between data and model outputs. The basic experiment curve is first presented in section 4.1 and Figure 4. Equations (7) and (9), described in sections 4.2 and 4.3, respectively, allow to deduce the NI and the SA for a given SW.
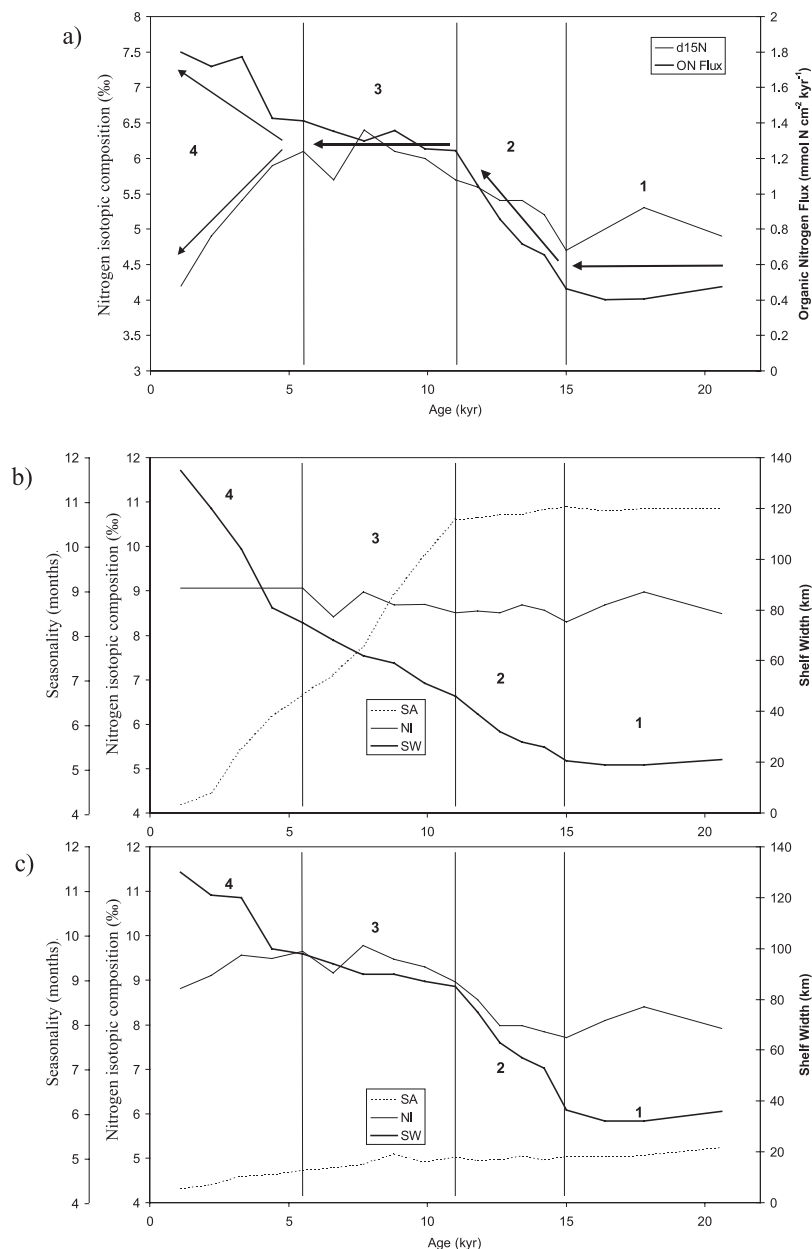
Figure 11. (a) Isotopic δ^{15}N signal (‰) and ONF (mmol N cm^{-2} kyr^{-1}) from the LGM to present for core 11K (21°28.87′N; 17°57.35′W; 1200 m depth). Data from *Martinez* [1997]. Reconstructed SW, SA, and NI for two different scenarios: (b) minimized nutrient input variations, and (c) more or less constant SA.

while the ONF continues to increase. We apply the previous equations (equations (7) and (9)) to these sedimentary data, choosing SW point by point. SA and NI are thus found as a function of age (kyr). Solutions are not unique, and two main scenarios appear.

[66] Figure 11b shows reconstructed parameters for the first scenario, in which we minimized the NI variations. For the first part of the curve, between 20 and 15 kyr, data of Figure 11a are reproduced by a configuration with a narrow shelf, which corresponds to the lowest sea level. Note that the reconstruction does not invoke a complete disappearance of the shelf. This is a weak point of our model, but it

can be explained. This can be interpreted by the fact that even without continental shelf the upwelling exists, and the organic matter accumulating on the continental slope has been advected by currents along the coast. This narrow SW is therefore "an equivalent" of organic matter production along the coast, rather than a real continental shelf production. The NI fluctuates around 8.6‰, and the SA is 11 months. This long SA period compensates for the low production of organic nitrogen in the narrow shelf configuration. The second part is characterized by an increase of the SW up to 46 km at 11 kyr and a relatively constant SA, varying between 10.5 and 11 months. During this period,

the NI remains almost constant. From 11 to 5.5 kyr, the SW increases up to 75 km, the SA decreases from 10.5 down to 6.6 months, and the NI increases slightly. Finally, from 5.5 to 1.1 kyr, the SW increases up to 135 km while the SA decreases to 4.5 months. The NI is then constant at 9.06‰. Changes in SW and SA explain how the ONF can increase while the sedimentary isotopic signal decreases. A low $\delta^{15}N$ signal is obtained by a large SW effect, and the corresponding high ONF is limited by a decrease in SA. The relationship between sedimentary $\delta^{15}N$ data and the reconstructed NI highlights two points. The first feature is the amplitude of variations of both data and reconstructions. The sedimentary $\delta^{15}N$ data presented here increase by 1.7‰ from 15 to 5.5 kyr, while the reconstructed NI only increases by 0.66‰. Between 5.5 and 1.1 kyr, the isotopic signal decreases by 1.9‰, while the reconstructed NI is constant. This means that, between 15 and 5.5 kyr, 60% (1.1‰) of the sedimentary isotopic signal variations could be explained by this local shelf immersion effect. The remaining 40% (0.66‰) of the recorded fluctuations may come from either the incoming nitrate isotopic signal or from variations in any postdepositional diagenetic process. The general trend in other cores is an increase of the $\delta^{15}N$ from glacial to interglacial and is explained by a modification in denitrification/nitrogen fixation ratio or nutrient supply. In our case, a strong increase is followed by a strong decrease of the $\delta^{15}N$ signal in core 11K from 5.5 to 1.1 kyr ($-1.9‰$). Because the general explanation involves an increase of this $\delta^{15}N$ signal, it cannot be used to explain as well the decrease observed locally. In our reconstructed scenario, this feature is completely reproduced by the shelf immersion effect, without invoking any external cause of variation. We therefore propose an explanation (the shelf immersion effect) that is valuable, at least locally, for both trends (increase followed by decrease $\delta^{15}N$).

[67] The second feature highlighted by this reconstruction is value of the NI itself. From 15 kyr to the present, the reconstructed NI varies between 8.3 and 9.06‰, which is different from the nutrient value of about 4.8‰ in the deep ocean [*Sigman et al.*, 2000]. To explain this difference of around 4‰, we may invoke either a higher local nitrate input $\delta^{15}N$ than this global mean, or a postdepositional diagenetic effect.

[68] In the Canary Islands region, *Freudenthal et al.* [2001] described a 4–5‰ increase of the $\delta^{15}N$ between the lower traps and the sediments. But the origin of this 4–5‰ shift is not clear because of a possible lateral advection effect. This isotopic enrichment between the sediment traps and the core sediments has been observed in many other areas [*Altabet and François*, 1994; *Francois et al.*, 1997]. Because this shift is constant with time, it will not influence down core variations in $\delta^{15}N$ [*Ganeshram et al.*, 2000; *Sigman et al.*, 2000]. Nevertheless, in this Mauritanian upwelling area, *Martinez et al.* [2000] did not find any significant N isotopic variation in core top sediments that could be attributed to diagenetic process. The existence of such an isotopic enrichment at the water-sediment interface or in the first centimeters of sediments, due to any diagenetic effect, is still an open question, which could explain part of the shift between the observed values and the
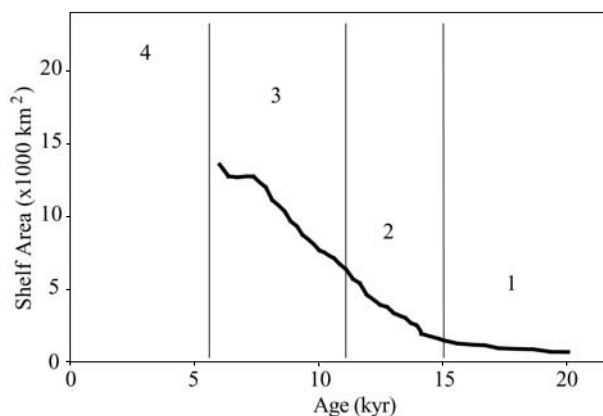

Figure 12. Evolution of the Mauritanian shelf area between 21.25°N and 23.25°N from the LGM to the climatic optimum. For each date, according to the corresponding sea level, the shelf area is defined as the area extending between the coast and the -100 m isodepth. Sea level data are from *Bard et al.* [1996].

reconstructed NI. Moreover, the sensitivity case study presented in section 5.4 will demonstrate that our model, by considering some slightly different fractionation factors, may be closer to realistic values of incoming $\delta^{15}NO_3^-$ and explain the fluctuations of the sedimentary isotopic signal by this local shelf immersion effect.

[69] The second scenario considers that the SA may not have changed along the glacial and interglacial periods. Figure 11c shows the SW and NI evolutions for a constant SA around 4–5 months. Before 15 kyr, the SW is already at 40 km, and increases rapidly to 85 km between 15 and 11 kyr. It increases slightly until 5.5 kyr, and reaches 130 km at 1.1 kyr. In this configuration, the $\delta^{15}N$ nitrate input that has to be invoked to reproduce the $\delta^{15}N$ data has much greater variations than for the previous scenario. These variations even exceed the sedimentary $\delta^{15}N$ fluctuations. The sedimentary isotopic signal drop from 5.5 kyr to the present would be therefore explained by a strong decrease of the NI signal. This is in contradiction with the general explanation of a denitrification increase in oxygen minimum layer areas, which would have made the global nitrate pool heavier. In each scenario, the reconstructed SWs vary between 20 and 130 km, whereas presently the continental shelf facing the location of the core 11K is only 40 km wide. This would confirm the fact that we have to include the upstream currents for the production of the sedimentary signal and not only what occurs at the same latitude than the core location.

[70] We still have to determine if the shelf area increases regularly (first scenario, Figure 11b) or with a rapid evolution between 15 and 11 kyr (second scenario, Figure 11c). Figure 12 shows how the shelf area evolves during the sea level rise from the LGM to 6 kyr. Because the shelf break is located at around 100 m depth in this region, the shelf area is defined as the area extending between the coast and the -100 m isobath. We considered the shelf included between 21.25°N (latitude of the core 11K location) and 23.25°N to integrate the upstream currents. This shelf evolution depicts
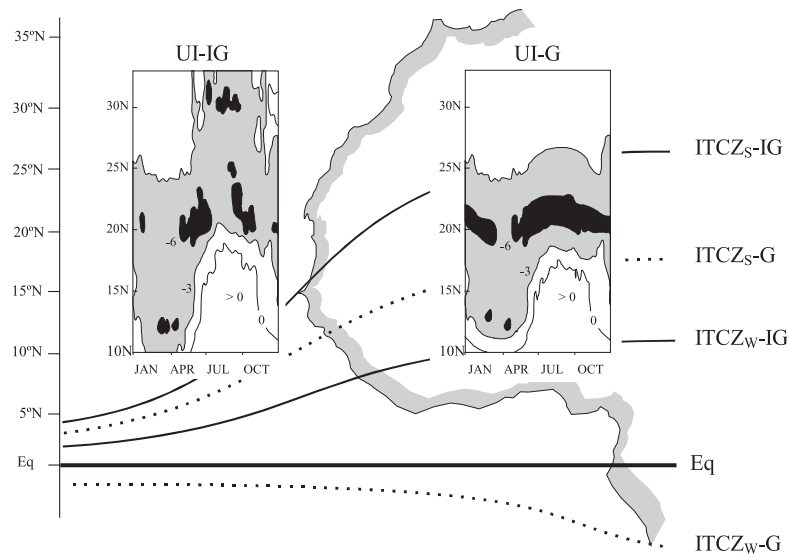
Figure 13. Relation between the UI and the ITCZ position on the Northwest African coast. The first panel represents the UI for interglacial (UI-IG), between 10°N and 35°N. This panel has been established for the period 1969–1976 by *Speth and Detlefsen* [1982]. This can be compared to the actual positions of the ITCZ in summer and winter (ITCZS-IG and ITCZW-IG, respectively, black lines). The second panel is a hypothetical map of the UI in the same area for the LGM (UI-G), constructed on the basis of previous map UI-IG, replacing the summer period by the spring-autumn feature. This can be related with the dashed lines on the background map, which represent the corresponding ITCZ position between summer (ITCZ$_S$-G) and winter (ITCZ$_W$-G) for the glacial period [adapted from *Leroux*, 1996].

a progressive and regular increase in surface area. This corresponds to and would confirm the first reconstructed scenario (Figure 11b).

[71] The sea level almost reaches its highest level around 5 kyr before present [*Fairbanks*, 1989; *Bard et al.*, 1996]. The shelf immersion therefore ends at this point. The continuing increase of the parameter SW of our scenarios between 5 kyr and the present should therefore correspond more to a climatic effect: changes in the wind intensity and/or direction can also change the extension of the upwelling area involved in the production of the organic matter arriving at the core location. The evolution of the SW happens concurrently with a changing SA, an indication of changing atmospheric forcing.

[72] This agreement with the first scenario would therefore confirm the existence of a higher SA during the LGM at Cape Blanc, which is discussed hereafter.

5.3. Interpretation of the SA Change

[73] The UI is defined as the sea surface temperature difference between coastal areas and the offshore zone. The greater this difference is, the stronger the upwelling (Figure 13). It can also be directly related to the wind system, with the seasonal variation of the UI related to the ITCZ migration. The seasonal latitudinal migration of the ITCZ induces a latitudinal change of the maximum upwelling location on the Northwest African coast (Figure 13), with amplifications of local coastline orientation effects. Between 20°N and 25°N, upwelling presently occurs throughout the year with a maximum intensity during autumn and spring [*Mit-*

telstaedt, 1991]. The optimal position of the wind system (dictated by the ITCZ position) for the upwelling at the core 11K location occurs during these two periods. It represents a duration of about 4–5 months.

[74] It has been proposed that the ITCZ migration may have changed in glacial periods [*Leroux*, 1993, 1996]. Its position would have been less northward in boreal summer and would have extended into the Southern Hemisphere during the boreal winter. The position of the ITCZ in boreal summer during the glacial period would therefore correspond to its present spring or autumn position. If the wind system of the present summer does not exist in glacial periods, a spring or autumn configuration would replace it. For the glacial boreal winter, no present equivalent exists, since the present ITCZ in our study area stays in the Northern Hemisphere.

[75] In Figure 13, a hypothetical UI map for the glacial period is proposed. The typical spring feature replaces the summer season. The wind regime may have been reduced, as compared to the present one. The glacial UI oscillation may include only two seasons: an extended period (spring-summer-autumn) favorable to upwelling and a short period (winter) unfavorable to upwelling. At Cape Blanc location (21°N), the upwelling maximum intensity would be therefore extended to 9–10 months or more. This could fit with our reconstruction, which yields the same SA, around 10.5 months, from 20 to 11 kyr (first scenario, Figure 11b).

5.4. Sensitivity to the Fractionation Parameters

[76] The sensitivity tests described previously in section 4.4 are applied to produce the sedimentary signal in the

same way. Figure 8 shows that the impact of different fractionation effects are almost equivalent for the different sea level situations. Only the range of the $\delta^{15}N$ is higher. As a consequence, the reconstruction of the sedimentary data by using these new curves produces the same kind of climatic scenario. In the case of a reduced fractionation factor associated with the nitrate uptake (3.2‰ instead of 5.2‰), the evolution of the parameters SA, NI, and SW is quite similar as previously described. Except for a few small differences, SW and SA have the same evolution than in the previous reconstruction. The small production associated with the short SW at the LGM is compensated by a long SA (around 11 months). The drop in this SA starts at the same period, at 11 kyr, to reach actual values (4−5 months).

[77] Because the sedimentary production modeled here is higher, and closer to the data values, the NI that has to be invoked is lower. It increases from 6.94 to 8.07‰ between 15 and 5.5 kyr, which represents an increase of 1.13‰, whereas the data increase is 1.7‰. For this part, the shelf immersion effect is less pronounced than before but is still a nonnegligible part of the signal variation. The strong decrease of the isotopic signal between 5.5 kyr and the present (−1.9‰) is reproduced by invoking only a small decrease of the NI (−0.21‰).

[78] The second sensitivity test is the addition of a fractionation factor associated with the remineralization loop. We have added a 1‰ fractionation. The increase of the $\delta^{15}N$ with the increase of the sea level is less pronounced than before. The increase of the data $\delta^{15}N$ (+1.7‰) is then reproduced by invoking a more variable NI (+1.2‰). But the second trend of the modeled output is well defined and entirely explains the $\delta^{15}N$ decrease observed in the data. The two cases of SA and SW are equivalent and yield the same interpretations.

[79] In conclusion, as shown in Figure 8, both sensitivity tests demonstrate that changing the fractionation factors has a strong impact on the sedimentary signal, all other parameters being equal. But the adjustment of these fractionation parameters improves our reconstructions by reducing the gap between the model outputs and the data. Most of all, it does not change the shape of this curve (Figure 4). This is the key point for the interpretation of the role of recycling on the shelf as a function of the SW, and to explain the decrease of the $\delta^{15}N$ signal between 5.5 kyr and the present. The shelf immersion effect stays an important factor to explain part of the sedimentary $\delta^{15}N$ variations. The effect of external causes is therefore diminished.

5.5. Reconstruction for Core 20bK

[80] The same reconstruction principle has been also applied to a second core off the Mauritanian upwelling. As we apply the same independent strategy for reconstruction for both cores, the resulting climatic scenarios can be fairly compared. Data of the core 20bK show a large variability in both nitrogen organic flux and nitrogen isotopic signal, but global trends can be described (Figure 14a). From 22 to 7 kyr, the ONF decreases from about 2.25 to 1 mmol N cm^{-2} kyr^{-1}. The sedimentary $\delta^{15}N$ slightly increases from 22 to 11 kyr, and then it swiftly increases from 5.83 to 7.81‰. The second part, from 11 to 7 kyr, oscillates around 7.5‰. Data are missing for the upper part of the core.

[81] The shelf effect described earlier results in two distinct trends: either increasing jointly the SW, the ONF, and the isotopic signal, or decreasing the isotopic signal with increasing ONF and increasing SW (Figure 4). The feature of the sedimentary core 20bK is a decrease of the ONF simultaneously with an increase of the $\delta^{15}N$ (Figures 9 and 14a). The best scenario we can reproduce is a constant SW, at about 80 km (Figure 14b). The ONF is then modulated by the SA, decreasing with oscillations from 8 to 3 months, and the isotopic signature results from the NI variations, between 7.5 and 10.5‰.

[82] For the present period, the reconstructed SW of 80 km necessary to explain the sedimentary signal means that the production facing the core location, i.e., where the continental shelf is about 150 km wide, is transported southward. For the glacial period, we also set a SW of about 80 km. It corresponds to the shelf that still exists northward of this location after the sea level decreases (Figure 6b).

[83] As a consequence of this constant SW, the SA and NI support the variations of the sedimentary signal. As for core 11K, the reconstruction leads to a decrease of the SA during the glacial-interglacial transition, but starts earlier at 16 kyr. The increase of the NI may come from a denitrification effect over the global ocean, but local effects are still possible. The 2D physical model we use does not allow us to consider some topographical accidents of the continental shelf. A few deep depressions exist on the shelf, near the coast (Figure 6). These topographic features may have an effect on the oceanic circulation, and thereby on the biological recycling. During the shelf immersion, these depressions may have led to sequestration, increasing the recycling of the biological food web, and therefore influencing the resulting $\delta^{15}N$ value. They may also act like a trap for the detritus, letting only the most offshore and isotopically heavier detritus to reach the continental slope. Such processes can only be described with a 3D physical model. Likewise, the reconstructed SA is a hypothesis to explain the decrease in ONF, which could be tested by running a 3D physical-biogeochemical model over 1 year, with different wind scenarios.

[84] Figure 15 summarizes the results of the reconstructions for both cores for three situations: present, 9, and 16 kyr. The three topographic maps, for each sea level situation, show clearly how the continental shelf disappears in front of core 11K for glacial periods, while it still exists in front of core 20bK. It also highlights that all the factors are important to explain the formation of the sedimentary signal (ONF and isotopic signal). Uncertainties about these reconstructed values are difficult to estimate, and would have to refer to the sensitivity studies about the fractionation factor. Most of all, this part is an attempt of reconstruction, showing a new method and some preliminary results.

[85] *Martinez et al.* [1999] interpreted the low glacial ONFes at the core 11K with upwelling-unfavorable wind conditions. This does not take into account that at a low sea level, without the possibility of continental shelf recirculation, the upwelling is less productive than for a high sea level, as we demonstrated in sections 3 and 4. On the contrary, we showed that a longer upwelling-favorable wind
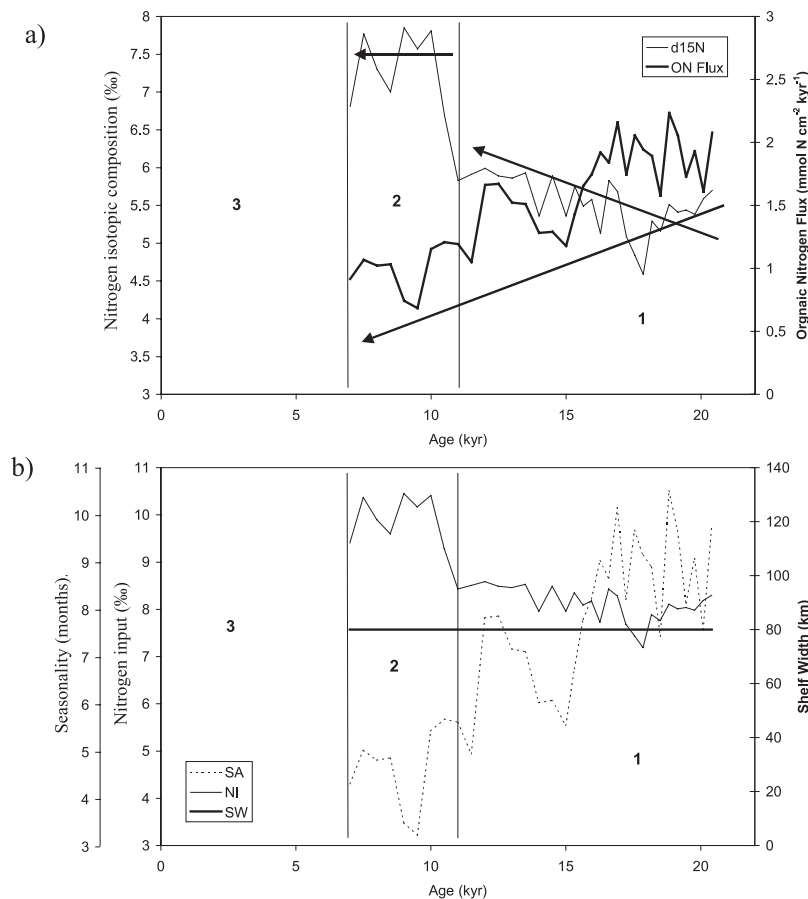
Figure 14. (a) Isotopic δ^{15}N signal (‰) and ONF (mmol N cm^{-2} kyr^{-1}) from the LGM to 7 kyr for core 20bK (25°1.7′N; 16°39.2′N; 1450 m depth). Data are from *Martinez* [1997]. (b) Reconstructed SW, SA, NI.

condition period is needed to compensate for the low productivity of the low sea level case. However, many studies propose an increased wind speed during the last glacial stage [*Martinez et al.*, 1999; *Matthewson et al.*, 1995; *Sarnthein et al.*, 1981; *Sicre et al.*, 2000]. The effect of this wind speed increase on the productivity in the low sea level case is uncertain and should be studied in further work.
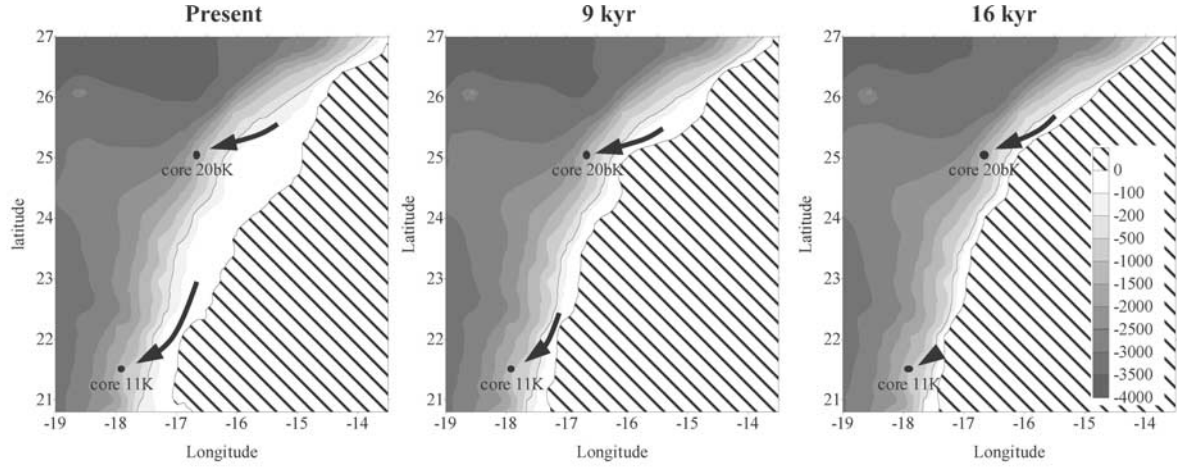
[86] The present study also invokes a small change in the δ^{15}N of the nitrate arriving in the Mauritanian upwelling area during the last deglaciation. In comparison, *Kienast* [2000] found no change in the δ^{15}N of the nitrate used during the primary production during the last climatic cycle in the South China Sea. Our results would confirm that the nitrogen budget over the global ocean could be more balanced than previously estimated. Major denitrification processes occurring in the North and southeast Pacific and the Indian Ocean, which affect the nitrate supply and N isotopic composition, may be counterbalanced by other processes affecting the nutrient content during their transfer through the rest of the ocean.

6. Conclusions

[87] Distinctions between both cores were made on the basis of the existence of a shelf in front of the core location

during the glacial or interglacial periods. We demonstrated that the SW is an important factor in explaining part of the sedimentary δ^{15}N signal and the ONF variations for the core 11K. Because the sea level rise from glacial to interglacial is an obvious fact, its local effect by the shelf immersion has to be taken into account in the formation and variations of the δ^{15}N signal. SA and NI, as well as other causes external to the upwelling area, like global patterns of denitrification/nitrogen fixation, are therefore secondary causes that modulate the signal. The upwelling SA may have been much higher during the LGM, around 11 months, due to a different seasonal ITCZ variation. For the core 11K, any sedimentary diagenetic process or any nitrogen loss/gain occurring in other ocean areas and affecting the nutrient isotopic signature would account for only 40% of the local sedimentary isotopic signal variations between 15 and 5.5 kyr. Between 5.5 kyr and the present, the sedimentary isotopic signal variations could be entirely reproduced by the local shelf immersion effect. For the core 20bK, the sedimentary signal is explained by a constant SW, coupled with a SA effect and a strong isotopic NI variation.

[88] Further investigations will be made with a 3D coupled physical-biogeochemical model to take into account the complex morphology of the present shelf,

Reconstructed parameters

	11K	20bK		11K	20bK		11K	20bK
Shelf Width	130 km	?		60 km	62 km		20 km	62 km
Seasonality	4.5 months	< 5 months		9 months	6 months		11 months	8 months
Nitrogen Input	9.0 ‰	?		8.6 ‰	10.1 ‰		8.6 ‰	8.36 ‰

Sedimentary core data

	11K	20bK		11K	20bK		11K	20bK
ONF	1.79	?		1.35	0.68		0.40	1.74
$\delta^{15}N$	4.20 ‰	?		6.10 ‰	7.57 ‰		5.0 ‰	5.13 ‰

Figure 15. Summary of the results: values of the reconstructed parameters (SW, SA, and NI) for both cores 11K and 20bK at three situations: present, 9, and 16 kyr. The bottom array summarizes the sedimentary core data. The ONF is expressed in (mmol N cm^{-2} kyr^{-1}). The maps represent the topography at each situation according to the sea level and shows the extension of the continental shelf (the line is the 200 m isodepth). The arrows represent the extension of the area of production of the organic matter reaching each core site. The question marks for core 20bK at present means that there is no sedimentary core data for this period, and that we cannot apply the model to reconstruct these values.

the current system (NE-SW), and the orientation of the wind relative to the coast determining the Ekman transport. This 3D configuration will also allow us to investigate the area of origin of the ONF found in the sedimentary core signal.

Appendix A: Photosynthesis and Grazing Expressions

[89] The following are the photosynthesis and grazing expressions. The photosynthesis growth rate is

$$J(z, t, N_N) = \min\left(J(z,t), J_{\max} \frac{N_N}{k_1 + N_N} \right).$$

The growth rate without nutrient limitation is

$$J(z,t) = \frac{J_{\max} \alpha I(z,t)}{\left[J_{\max}^2 + (\alpha I(z,t))^2 \right]^{1/2}}.$$

The maximum growth rate is

$$J_{\max} = ab^{cT}.$$

Insolation is shown by

$$I(z,t) = I(t)_{z=0} \exp\left(\frac{(k_w z + k_c \int_0^z N_P \, dz)}{\sqrt{1 - (\cos\theta/1.33)^2}} \right).$$

The zooplankton grazing expression is

$$G(N_P) = \frac{g\varepsilon N_P^2}{g + \varepsilon N_P^2},$$

where min (x, y) is the function "minimum," z is depth, t is time, T is temperature (°C), and θ is the angle of incidence at noon (in radian).

References

Alldredge, A. L., and C. Gotschalk, In situ settling behavior of marine snow, *Limnol. Oceanogr.*, 33, 339–351, 1988.

Allen, J. S., P. A. Newberger, and J. Federiuk, Upwelling circulation on the Oregon continental shelf, part I. Response to idealized forcing, *J. Phys. Oceanogr.*, 25, 1843–1866, 1995.

Altabet, M. A., and W. B. Curry, Testing models of past ocean chemistry using foraminifera $^{15}N/^{14}N$, *Global Biogeochem. Cycles*, 3, 107–119, 1989.

Altabet, M. A., and R. François, Sedimentary nitrogen isotopic ratio as a recorder for surface ocean nitrate utilization, *Global Biogeochem. Cycles*, 8, 103–116, 1994.

Altabet, M. A., R. François, D. W. Murray, and W. L. Prell, Climate-related variations in denitrification in the Arabian Sea from sediment $^{15}N/^{14}N$ ratios, *Nature*, 373, 506–509, 1995.

Altabet, M. A., M. J. Higginson, and D. W. Murray, The effect of millennial-scale changes in Arabian Sea denitrification on atmospheric CO_2, *Nature*, 415, 159–162, 2002.

Babin, M., A. Morel, H. Claustre, A. Bricaud, Z. Kolber, and P. G. Falkowski, Nitrogen- and irradiance-dependent variations of the maximum quantum yield of carbon fixation in eutrophic, mesotrophic and oligotrophic marine systems, *Deep Sea Res., Part I*, 43(8), 1241–1272, 1996.

Bard, E., B. Hamelin, M. Arnold, L. Montaggioni, G. Cabioch, G. Faure, and F. Rougerie, Deglacial sea-level record from Tahiti and the timing of global meltwater discharge, *Nature*, 382, 241–244, 1996.

Bertrand, P., T. F. Pedersen, P. Martinez, S. Calvert, and G. Shimmield, Sea level impact on nutrient cycling in coastal upwelling areas during deglaciation: Evidence from nitrogen isotopes, *Global Biogeochem. Cycles*, 14, 341–355, 2000.

Blumberg, A. F., and G. L. Mellor, Diagnostic and prognostic numerical circulation studies of the South Atlantic Bight, *J. Geophys. Res.*, 88(C8), 4579–4592, 1983.

Blumberg, A. F., and G. L. Mellor, A description of a three-dimensional coastal ocean circulation model, in *Three-Dimensional Coastal Ocean Models*, *Coastal Estuarine Ser.*, vol. 4, edited by N. Heaps, 208 pp., AGU, Washington, D.C., 1987.

Calvert, S. E., B. Nielsen, and M. R. Fontugne, Evidence from nitrogen isotope ratios for enhanced productivity during formation of eastern Mediterranean sapropels, *Nature*, 359, 223–225, 1992.

Calvert, S. E., C. A. Baturin-Pollock, J. W. Farrell, R. S. Ganeshram, T. F. Pedersen, N. A. D. Waser, and J.-P. Wu, Nitrogen isotope ratios in sedimentary organic matter as a proxy for nutrient utilization and palaeoproductivity, in *Organic Geochemistry: Developments and Applications to Energy, Climate, Environment and Human History. Selected Papers From the 17th International Meeting on Organic Geochemistry, 4th–8th September 1995*, edited by J. O. Grimalt and C. Dorronsoro, pp. 880–881, AIGOA, Donostia-San Sebastián, Spain, 1995.

DeNiro, M. J., and S. Epstein, Influence of diet on the distribution of nitrogen isotopes in animals, *Geochim. Cosmochim. Acta*, 45, 341–351, 1980.

Emmer, E., and R. C. Thunell, Nitrogen isotope variations in Santa Barbara Basin sediments: Implications for denitrification in the eastern tropical North Pacific during the last 50,000 years, *Paleoceanography*, 15, 377–387, 2000.

Evans, G., The role of local models and data sets in the Joint Global Ocean Flux Study, *Deep. Sea Res., Ser. I*, 46, 1369–1389, 1999.

Fairbanks, R. G., A 17,000-year glacio-eustatic sea level record: Influence of the glacial melting rates on the Younger Dryas event and deep-ocean circulation, *Nature*, 342, 637–642, 1989.

Falkowski, P. G., Evolution of the nitrogen cycle and its influence on the biological sequestration of CO_2 in the ocean, *Nature*, 387, 272–275, 1997.

Farrell, J. W., T. F. Pedersen, S. E. Calvert, and B. Nielsen, Glacial-interglacial changes in nutrient utilization in the equatorial Pacific Ocean, *Nature*, 377, 514–517, 1995.

Fasham, M. R. J., Variations in the seasonal cycle of biological production in subarctic oceans: A model sensitivity analysis, *Deep Sea Res., Part I*, 42, 1111–1149, 1995.

Fischer, G., B. Donner, V. Ratmeyer, R. Davenport, and G. Wefer, Distinct year-to-year particle flux variations off Cape Blanc during 1988–1991: Relation to $\delta^{18}O$-deduced sea-surface temperatures and trade winds, *J. Mar. Res.*, 54, 73–98, 1996.

François, R., M. A. Altabet, and L. H. Burckle, Glacial to interglacial changes in surface nitrate utilization in the Indian sector of the Southern Ocean as recorded by sediment $\delta^{15}N$, *Paleoceanography*, 7, 589–606, 1992.

Francois, R., M. A. Altabet, E. F. Yu, D. M. Sigman, M. P. Bacon, M. Frank, G. Bohrmann, G. Bareille, and L. D. Labeyrie, Contribution of Southern Ocean surface-water stratification to low atmospheric CO_2 concentrations during the last glacial period, *Nature*, 389, 929–935, 1997.

Freudenthal, T., S. Neuer, H. Meggers, R. Davenport, and G. Wefer, Influence of lateral particle advection and organic matter degradation on sediment accumulation and stable nitrogen isotope ratios along a productivity gradient in the Canary Islands region, *Mar. Geol.*, 177, 93–109, 2001.

Fütterer, D. K., The modern upwelling record off Northwest Africa, in *Coastal Upwelling: Its Sedimentary Record, Part B: Sedimentary Records of Ancient Coastal Upwelling*, edited by J. Tiede and E. Süess, pp. 105–121, Plenum, New York, 1983.

Gabric, A. J., L. Garcia, L. Van Camp, L. Nykjaer, W. Eifler, and W. Schrimpf, Offshore export of shelf production in the Cape Blanc (Mauritania) giant filament as derived from coastal zone color scanner imagery, *J. Geophys. Res.*, 98(C3), 4697–4712, 1993.

Ganeshram, R. S., et al., Large changes in oceanic nutrient inventories from glacial to interglacial periods, *Nature*, 376, 755–758, 1995.

Ganeshram, R. S., T. F. Pedersen, S. E. Calvert, G. W. McNeill, and M. R. Fontugne, Glacial-interglacial variability in denitrification in the world's oceans: Causes and consequences, *Paleoceanography*, 15, 361–376, 2000.

Ganeshram, R. S., T. F. Pedersen, S. E. Calvert, and R. Francois, Reduced nitrogen fixation in the glacial ocean inferred from changes in marine nitrogen and phosphorus inventories, *Nature*, 415, 156–159, 2002.

Giraud, X., P. Bertrand, V. Garçon, and I. Dadou, Modeling $\delta^{15}N$ evolution: First palaeoceanographic applications in a coastal upwelling system, *J. Mar. Res.*, 58, 609–630, 2000.

Gunson, J., A. Oschlies, and V. Garçon, Sensitivity of ecosystem parameters to simulated satellite ocean color data using a coupled physical-biological model of the North Atlantic, *J. Mar. Res.*, 57, 613–639, 1999.

Holmes, M. E., P. J. Müller, R. R. Schneider, M. Segl, J. Pätzold, and G. Wefer, Stable nitrogen isotopes in Angola Basin surface sediments, *Mar. Geol.*, 134, 1–12, 1996.

Holmes, M. E., P. J. Müller, R. R. Schneider, M. Segl, and G. Wefer, Spatial variations in euphotic zone nitrate utilization based on $\delta^{15}N$ in surface sediments, *Geo Mar. Lett.*, 18(1), 58–65, 1998.

Kienast, M., Unchanged nitrogen isotopic composition of organic matter in the South China Sea during the last climatic cycle: Global implications, *Paleoceanography*, 15, 244–253, 2000.

Leroux, M., The mobile polar high: A new concept explaining present mechanisms of meridional airmass and energy exchanges and global propagation of palaeoclimatic changes, *Global Planet. Change*, 7, 69–93, 1993.

Leroux, M., *La Dynamique du Temps et du Climat*, 310 pp., Masson, Paris, 1996.

Liu, K.-K., and I. R. Kaplan, The eastern tropical Pacific as a source of ^{15}N-enriched nitrate in seawater off southern California, *Limnol. Oceanogr.*, 34, 820–830, 1989.

Martinez, P., Paléoproductivités du système d'upwellings nord-ouest africain et variations climatiques au cours du Quaternaire terminal, Ph.D. thesis, Univ. of Bordeaux, Talence, France, 1997.

Martinez, P., P. Bertrand, G. B. Shimmield, K. Cochrane, F. J. Jorissen, J. Foster, and M. Dignan, Upwelling intensity and ocean productivity changes off Cape Blanc (Northwest Africa) during the last 70,000 years: Geochemical and micropalaeontological evidence, *Mar. Geol.*, 158, 57–74, 1999.

Martinez, P., P. Bertrand, S. E. Calvert, T. F. Pedersen, G. B. Shimmield, E. Lallier-Verges, and M. R. Fontugne, Spatial variations in nutrient utilization, production and diagenesis in the sediments of a coastal upwelling

regime (NW Africa): Implications for the paleoceanographic record, *J. Mar. Res.*, *58*, 809–835, 2000.

Matthewson, A. P., G. B. Shimmield, D. Kroon, and A. E. Fallick, A 300 kyr high-resolution aridity record of the North African continent, *Paleoceanography*, *10*, 677–692, 1995.

Mellor, G. L., *User's Guide for a Three-Dimensional, Primitive Equation, Numerical Ocean Model*, 41 pp., Princeton Univ. Press, Princeton, N.J., 1998.

Mellor, G. L., and T. Yamada, Development of a turbulence closure model for geophysical fluid problems, *Rev. Geophys.*, *20*(4), 851–875, 1982.

Minagawa, M., and E. Wada, Stepwise enrichment of ^{15}N along food chains: Further evidence and relation between δ^{15}N and animal age, *Geochim. Cosmochim. Acta*, *48*, 1135–1140, 1984.

Minas, H. J., L. A. Codispoti, and R. C. Dugdale, An analysis of production-regeneration system in the coastal upwelling area off NW Africa based on oxygen, nitrate and ammonium distributions, *J. Mar. Res.*, *40*, 615–641, 1982.

Mittelstaedt, E., The ocean boundary along the Northwest Africa coast: Circulation and oceanographic properties at the sea surface, *Prog. Oceanogr.*, *26*, 307–355, 1991.

Montoya, P., Nitrogen isotope fractionation in the modern ocean: Implication for sedimentary record, in *Carbon Cycling in the Glacial Ocean: Constraints on the Ocean's Role in Global Change*, edited by R. Zahn, pp. 259–279, Springer-Verlag, New York, 1994.

Morel, A., Process studies in eutrophic, mesotrophic and oligotrophic oceanic regimes within the tropical northeast Atlantic, in *The Changing Ocean Carbon Cycle: A Midterm Synthesis of the Joint Global Ocean Flux Study*, edited by R. B. Hanson, H. W. Ducklow, and J. G. Field, pp. 338–374, Cambridge Univ. Press, New York, 2000.

Oschlies, A., and V. Garçon, An eddy-permitting coupled physical-biological model of the North Atlantic: 1. Sensitivity to advection numerics and mixed layer physics, *Global Biogeochem. Cycles*, *13*, 135–160, 1999.

Sarmiento, J. L., R. D. Slater, M. J. R. Fasham, H. W. Ducklow, J. R. Toggweiler, and G. T. Evans, A seasonal three-dimensional ecosystem model of nitrogen cycling in the North Atlantic euphotic zone, *Global Biogeochem. Cycles*, *7*, 417–450, 1993.

Sarnthein, M., G. Tetzlaff, B. Koopmann, K. Wolter, and U. Pflaumann, Glacial and inter-glacial wind regimes over the eastern sub-tropical Atlantic and Northwest Africa, *Nature*, *293*, 193–196, 1981.

Sicre, M. A., Y. Ternois, M. Paterne, A. Boireau, L. Beaufort, P. Martinez, and P. Bertrand, Biomarker stratigraphic records over the last 150 kyears off the NW African coast at 25 degrees N, *Org. Geochem.*, *31*(6), 577–588, 2000.

Sigman, D. M., M. A. Altabet, D. C. McCorkle, R. Francois, and G. Fischer, The δ^{15}N of nitrate in the Southern Ocean: Consumption of nitrate in surface waters, *Global Biogeochem. Cycles*, *13*, 1149–1166, 1999.

Sigman, D. M., M. A. Altabet, D. C. McCorkle, R. Francois, and G. Fischer, The δ^{15}N of nitrate in the Southern Ocean: Nitrogen cycling and circulation in the ocean interior, *J. Geophys. Res.*, *105*(C8), 19,599–19,614, 2000.

Speth, P., and H. Detlefsen, Meteorological influences on upwelling off northwest Africa, in *Rapports et Procès-verbaux des Réunions*, *Rep. 180*, pp. 29–34, Intl. Counc. for the Explor. of the Sea, Copenhagen, 1982.

Steele, J. H., and E. W. Hederson, The role of predation in plankton models, *J. Plankton Res.*, *14*, 157–172, 1992.

Waser, N. A. D., P. J. Harrison, B. Nielsen, S. E. Calvert, and D. H. Turpin, Nitrogen isotope fractionation during the uptake and assimilation of nitrate, nitrite, ammonium and urea by a marine diatom, *Limnol. Oceanogr.*, *43*, 215–224, 1998.

Wefer, G., and G. Fischer, Seasonal patterns of vertical particle flux in equatorial and coastal upwelling areas of the eastern Atlantic, *Deep Sea Res., Part I*, *40*, 1613–1645, 1993.

————————————

P. Bertrand, Départment de Géologie et Océanographie, UMR 5805 EPOC, CNRS, Université Bordeaux I, 33405 Talence Cedex, France.

I. Dadou and V. Garçon, LEGOS, CNRS UMR 5566, 18 Avenue Edouard Belin, 31401 Toulouse Cedex 4, France.

X. Giraud, Max Planck Institute for Biogeochemistry, Winzerlaerstrasse 10, 07745 Jena, Germany. (xgiraud@bgc-jena.mpg.de)